Exp Fluids (2011) 50:397–406
DOI 10.1007/s00348-010-0941-x

RESEARCH ARTICLE

Vortex dipolar structures in a rigid model of the larynx at flow onset

N. E. Chisari · G. Artana · D. Sciamarella

Received: 14 September 2009 / Revised: 26 June 2010 / Accepted: 13 July 2010 / Published online: 3 August 2010

Abstract Starting jet airflow is investigated in a channel with a pair of consecutive slitted constrictions approximating the true and false vocal folds in the human larynx. The flow is visualized using the Schlieren optical technique and simulated by solving the Navier-Stokes equations for an incompressible two-dimensional viscous flow. Laboratory and numerical experiments show the spontaneous formation of three different classes of vortex dipolar structures in several regions of the laryngeal profile under conditions that may be assimilated to those of voice onset.

1 Introduction

The dynamics of the jet traversing the glottis in the larynx is the subject of active research, particularly since powerful experimental and numerical tools are available to gain insight into the role that the evolution of flow patterns in the larynx might have in vocal production.

N. E. Chisari · G. Artana
LFD, Facultad de Ingeniería, Universidad de Buenos Aires,
Av. Paseo Colón 850, C1063ACV Buenos Aires, Argentina

G. Artana
e-mail: gartana@fi.uba.ar

Present Address:
N. E. Chisari
Department of Astrophysical Sciences, Princeton University,
08544 Princeton, NJ, USA
e-mail: nchisari@princeton.edu

D. Sciamarella (✉)
LIMSI-CNRS, Bâtiment 508, 91403 Orsay, France
e-mail: sciamarella@limsi.fr

Highly performant flow visualization and measurement techniques such as particle image velocimetry are currently being applied to in vivo and in vitro experiments designed to study the laryngeal jet (Triep et al. 2005; Erath and Plesniak 2006, 2006; Khosla et al. 2007). Schlieren flow visualization (Settles 2001) is particularly interesting because it is non-intrusive and does not require any seeding of the flow with particles. This technique is common in musical acoustics and has been successfully used to study jet formation and evolution of vortex pairs in the mouth of a recorder (Verge et al. 1994).

Other examples of the use of Schlieren or gas injection for flow visualization in musical acoustics can be found in the seminal work of Cremer (1967) and more recently in Paál et al. (2006). In the context of speech production, the Schlieren system has been used to provide evidence on the issue of flow separation in the phonation process (Pelorson et al. 1994) and to study a glottal-like starting jet in a channel with a single-slitted constriction (Hofmans 1998). The latter includes Schlieren stroboscopic photography, hot wire anemometry and two-dimensional numerical simulations of the flow in half the channel (hemi-larynx), with symmetry boundary conditions imposed across the glottal midline.

In this paper, we study the dynamics of a jet in a channel with two consecutive slitted constrictions roughly representing the true and the false vocal folds in the larynx, within the time ranges that are compatible with phonation onset. This kind of geometry has been used as a first step model in several experimental studies of laryngeal flow behavior (Kucinschi et al. 2006). The model that we use is directly inspired in experiments designed to study the influence of a constriction in the near field of the vocal folds (Bailly et al. 2008). Flow visualizations in our laboratory experiments are performed with a Schlieren system

and recorded using high-speed imaging. Our numerical experiments consist in Direct Numerical Simulations (DNS) of two-dimensional (2D) flow in the full channel, in order to capture possible flow asymmetries.

The article is organized as follows. The following two sections provide a brief background on the function of the structures in the larynx and on the theory of vortex dipoles. Section 5 is devoted to describe the laboratory and numerical experiments. An integrated account of the results is provided in Sect. 4. Conclusions are surveyed in the last section.

2 The target problem

The larynx has two sets of interior folds: the vocal folds, endowed with a structure that makes them good biomechanical oscillators, and the 'false vocal folds' (also called 'ventricular bands' or 'vestibular folds') which are a pair of mucous structures, rarely capable of vibrating (Fig. 1). The glottis is the space between the vocal folds and has the form of a narrow slit when the vocal folds are adducted. The ventricular bands are wedge-shaped tissues that define behind them a kind of 'basin' known as the laryngeal ventricle or 'Morgani's ventricle'. The size of this ventricle (determined by the false vocal fold height, gap and aperture) remains speculative, since the mechanisms of false vocal fold positioning are unclear. However, it is agreed that the false vocal folds have a tendency to adduct toward the midline during both normal and abnormal phonation. Laminagraphic X-ray tracings and CT scans have helped characterize the geometry of the larynx in voice production (Agarwal et al. 2003; Zheng et al. 2009). For the purposes of this article, the larynx is roughly assimilated to a slit (the glottis), followed by a ventricle whose shape is defined by the position of the ventricular bands.

During voice production, this geometry is not static: the vocal folds vibrate modulating the incoming subglottal flow. In experimental essays, a natural substitute for the self-oscillating folds is a pulsatile flow through a rigid model of the larynx. Such a configuration is less realistic but easier to control (e.g. Erath and Plesniak 2006). Some of these studies include the false vocal folds in order to elucidate their aerodynamic impact, which is supposed to be relevant in certain cases.

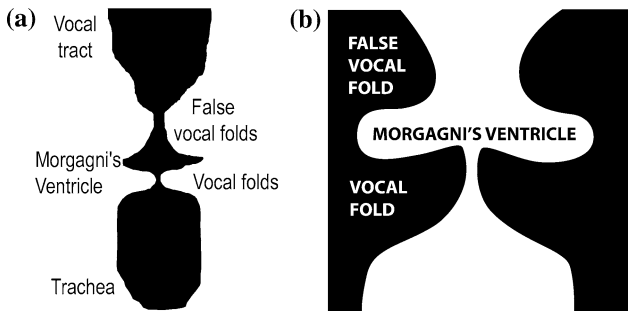

Fig. 1 Geometric profile of the larynx **a** traced from a CT scan of a normal human larynx (Zheng et al. 2009), **b** with the shape of laminagraphic tracings in Agarwal et al. (2003)

At voice onset, the air from the lungs flows through the adducted true and false vocal folds toward the vocal tract. Due to the slitted form of the glottis, associated with a contraction ratio of order 10^{-2}, laryngeal flow is often considered planar or quasi-2D (Vilain 2002). Recent visualization experiments in geometries devoid of ventricular bands (Neubauer et al. 2007) indicate that the quasi-2D nature of the near field which emanates from the glottis will soon be destroyed by three dimensional (3D) instabilities when the vocal folds oscillate. Experiments using a water loop facility and motor-driven silicone models of the vocal folds with static ventricular bands (Triep et al. 2005) also contend that the 2D structures formed in the human larynx during phonation are short lived. In this study, the working fluid is air, the model is a set of two aligned consecutive slits, and the focus is upon the early stages of flow evolution ($\sim$10 ms).

3 Background on vortex dipoles

The doubly constricted channel of the larynx possesses geometrical restrictive conditions favoring the roll-up of counter-rotating vortex structures as the jet is formed at the slits. Doubly constricted channels are also relevant in the case of whistling (Wilson et al. 1971), where the two consecutive constrictions have a circular rather than a slitted geometry. Whistling of slits is studied in Billon et al. (2005) and Glesser et al. (2008). Where circular nozzles produce *vortex rings*, slitted nozzles produce a stretched structure along the slit direction, in which the predominant pattern is a compact (quasi-)2D flow pack of two counter-rotating circulations with an advective interaction between them. This flow pattern has been termed *vortex dipole*. The alternative expression *vortex pair* is generally reserved for the case of co-rotating vortices.

The usage of the term 'dipole' may be confusing in the context of sound production, where the reference to acoustical multipoles is commonplace. Mathematically, acoustical dipoles are 'true dipoles' in the sense that they refer to a part of a multipolar spatial expansion of a field, while this is not necessarily the case for the vortex pattern that we attempt to describe. Multipolar expansions are also used in vortex dynamics, and thus the expression 'vortex dipole' is something of a misnomer. Yet, and because the term is chosen as keyword in the literature that has inspired

the analysis of the results presented in this work, let us hereafter use the terms 'vortex dipole' and 'vortex dipolar structure' interchangeably, to refer to a pattern with a counter-rotating vortex pair. Let us also remark that vortex sound generation, which is extensively discussed in Howe (1998, 2003, 2007), is not being addressed in this paper.

Many experimental studies on the formation and evolution of vortex dipoles use a specific physical mechanism to suppress the spanwise motion and thus guarantee the two-dimensionality of the flow. Such mechanisms are increasingly effective as the formed dipolar structures develop, making them particularly persistent. This occurs in nature with background rotation or density stratification, which explains why this concept is pervasive in oceanography or atmospheric sciences. But quasi-2D flow can also occur due to geometrical factors as those for flow in thin layers, shallow water, soap films or slitted nozzles. Contamination by 3D effects in our experimental setup is limited by a twofold condition: the aligned double-slit geometry (in space), and the focus on the early stages of the flow (in time).

When a jet from a nozzle is used to generate vortex dipoles, the vortices together with the jet between them are said to constitute a *starting vortex dipole*. In spite of the differences in experimental conditions, some aspects of the behavior of the vortex dipolar structure at the head of the jet found in the experiments that we present in the following section can be described with the model proposed by Afanasyev in (2006).

Starting vortex dipoles do not necessarily admit a model in terms of a stable head followed by a quasi-steady tail. The system formed by the trailing jet and the leading dipolar structure can be subject to instabilities. There are two types of instability modes in a plane jet that can be assimilated to the ones in a trailing plane jet: a varicose mode, with symmetric swellings and contractions with respect to the jet centerline, and a sinuous mode, where the instability waves present antisymmetrical undulations with respect to the jet centerline (Huang and Hsiao 2006). The trailing jet may also behave as a *sequential* vortex dipole generator (Liepmann and Gharib 1992), and when several vortex dipoles move along a common axis, the rearward dipole tends to become smaller and move faster than the forward one. Due to their mutual interaction, the former can then pass (or leapfrog) through the latter and merge (or coalesce) with it. Such a phenomenon is known as leapfrogging. This kind of coaxial interactions, described by Hofmans (1998) as pairing and merging events between secondary vortices, has been reported in the single-slit case. Notice that in the case that we study, switching between the two instability modes of the planar trailing jet can perturb the trajectory of the vortex dipolar structures associated with it.

Creation of intense vortex dipoles can also occur due to the interaction of vorticity with non-slip boundaries. In general, when a vortex approaches a non-slip wall, it induces a thin vorticity layer that rolls up on itself and gives birth to a vortex, which is interpreted as the *rebound* of the first one (Orlandi 1990). Rebounding vortex dipoles may have sufficient circulation to induce on themselves a motion in the opposite direction to the motion of the incident vortex dipole. Our results will illustrate many of these effects.

4 Laboratory and numerical experiments

4.1 Experimental setup

Fixed rigid models have been used with the purpose of studying unsteady flow through the glottis (Kucinschi et al. 2006; Hofmans et al. 2003; Deverge et al. 2003). The double slit version of the model that we take up (Bailly et al. 2008) has been used to assess the influence of the false vocal folds. Our experimental setup is made up of four main parts: a double-slit model of the larynx, a pneumatic circuit for air supply, an optical system for flow visualization, and a system for Helium injection.

An aluminium cylindrical tube with a diameter of 25 mm and a length of 80 cm is used at the place of the trachea. This tube is connected to a square-sectioned channel representing the larynx. For the visualization purposes, the channel has a square cross-section with two of the lateral sides built from a sheet of 2 mm-thick float glass. The other two sides of the channel are built in acrylic glass (PMMA). At the place of the vocal folds stands a pair of pieces of 25-mm-thick PMMA with semi-cylinders having a 5-mm radius of curvature. Above them, a second pair of PMMA liplike round structures of the same dimensions define the constriction representing the false vocal folds. The two constrictions are separated by a distance L, with default values of either 10 or 20 mm (see Fig. 2). The separation of the first pair of semi-cylinders determines the width of the first slit representing the glottis: $h_1 = 1$ mm is the default value. With this configuration,

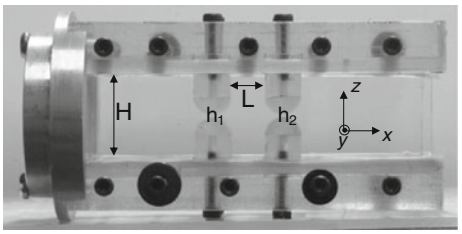

Fig. 2 The simplified double-slit laryngeal model built for the laboratory experiments

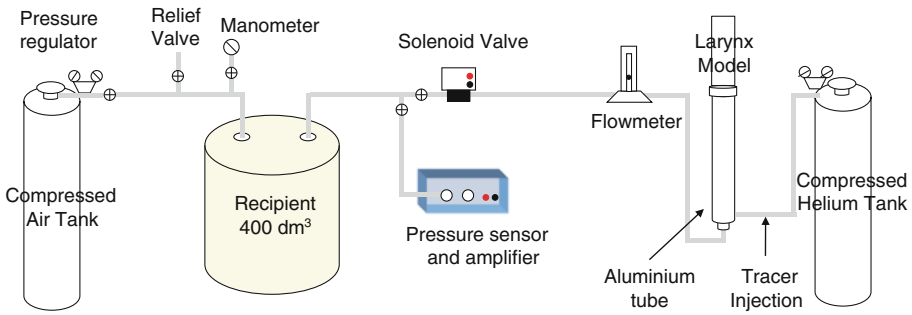

Fig. 3 Diagram of the pneumatic circuit with tracer injection system (not in scale)

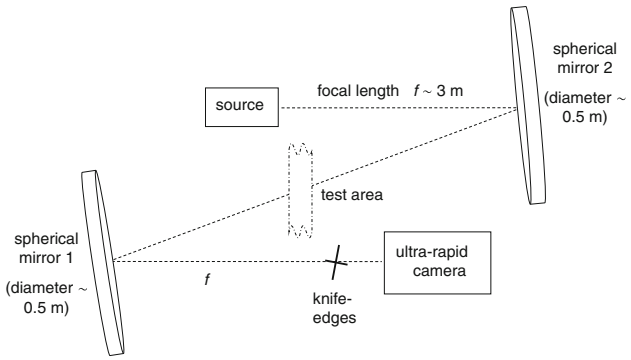

Fig. 4 Diagram of the $Z-$ type Schlieren system

the first slit has a contraction ratio of 25:1. The aperture h_2 of the second slit, representing the false vocal fold gap, is adjustable: we have performed experiments with a second-slit width of 1, 2, 4 and 6 mm.

The pneumatic circuit, sketched in Fig. 3, supplies the model with air at a regulated flow rate so that the velocity through the first slit reaches velocities comparable to the typical velocities through the glottis. A compressed dry air tank feeds a 400 dm^3 sealed recipient. A valve and pipe system connected to a manometer are employed to measure the pressure in the tank as it builds up and reaches the optimal value. When the desired pressure is attained, the feeding is closed and a solenoidal two-way valve opens up to release the air into the circuit. The solenoid valve has a fixed time response of 5 ms guaranteed by the manufacturer. Activating the valve to open the circuit every time a measurement is made assures the repeatability of the experiment. A floating-ball flowmeter inserted before the model measures the airflow through the system in steady flow conditions (past the initial transient) with an accuracy of 0.5 l/min. This flowrate fixes the Reynolds number of the experiment past the opening transient, which is set to attain values close to 1,000. The larynx model is positioned so that the air flows upwards through the double slit.

The flow is visualized with a Z-type Schlieren system, shown in Fig. 4, formed by two 0.5 m-diameter 3 m-focal length spherical mirrors. The illumination source consists of a light bulb, its light concentrated by a lens upon an optical-quality diffuser. A square slit of adjustable size is placed at the focus of the first mirror in order to generate a parallel beam. The larynx model is mounted so that this parallel beam is oriented in the direction of the slits length (the direction labeled y in Fig. 2). The index of refraction gradients produced in between deviate the parallel light rays, causing a pattern of shadows in an otherwise smooth background. Light collected by the second mirror is focused on a pair of knife edges at the stigmatic focuses of the second mirror. The partial obstruction of the image by the knife edges enhances contrast. As the airflow passes through the slits, an ultra-rapid CMOS camera records the pattern formed by the transparent flow. Frames are recorded at frequencies from 800 to 2,000 frames/s.

Pure Helium gas is injected as a tracer. A pressure regulator at the exit of the Helium tank allows to adjust the line pressure of the tubing (2 mm in diameter) that connects the Helium tank with the aluminium tube representing the trachea. Helium is injected into the base of the aluminium tube through a circular 2-mm orifice, at about 80 cm from the first slit of the larynx model. During the tests, and before triggering the airflow with the solenoid valve, the regulator is adjusted at a pressure that is slightly higher than the atmospheric pressure. The value of the Helium pressure regulator is then kept constant during each experiment. When the solenoid valve is opened, a flow through the model of a dilute mixture of Helium and air takes place. This flow produces a non-uniform distribution of Helium concentration that allows the observation of the vortical structures at the slits of the model that we study in this work. The large focal distance of the Schlieren mirrors and the blocking of the source image at the focus with the knife edge are parameters that make the optical system highly sensitive to concentration gradients. If Helium injection is not properly tuned, saturated images are produced. Images with a good contrast are obtained only when the flow mixture of air and Helium contains sufficiently low rates of Helium. This assures that the air properties are only slightly perturbed.

Notice that the Schlieren technique (as used here) does not isolate 2D (x, z) slices of the flow through the double slit, but accumulates the optical effects along the slits

direction (y). Thus, the possibility of identifying flow patterns in our Schlieren images relies on a certain spatial coherence of the flow in y, which ensures that the quasi-two-dimensionality of the flow has not been seriously degraded. Within the time ranges that we inspect, the position of the second slit in the model helps restoring the two-dimensionality of the flow at a 'safe' distance from the first slit. This explains why pattern recognition with this visualization setup is not hindered by typical 3D phenomena in non-circular jets (Gutmark and Grinstein 1999).

4.2 Numerical method

The numerical technique consists of a multigrid finite-difference Navier-Stokes solver implemented to simulate unsteady airflow through a 2D channel with fixed or moving boundaries. This code has been previously used to solve for unsteady glottal airflow with immersed moving boundaries. For details on the numerical method, the reader is referred to Sciamarella and Le Quéré (2008).

In the numerical experiments performed in this work, the code settings are adapted to the laboratory experiments. The boundary geometry of the doubly constricted channel (defined by h_1, h_2 and L) is set at the beginning of the numerical experiment. The prototype configuration has $h_1 = 1$ mm, $h_2 = 2$ mm, $L = 20$ mm. The time dependence of the incoming velocity U_{in} is supposed to be constant except for the first 5 ms response of the solenoid valve. The value of the constant is established in correspondence with the value indicated by the flowmeter of the experimental setup at large times. The Reynolds number is built on the channel's maximum height H and on the constant value of the incoming velocity. In order to reproduce the opening maneuver of the solenoid valve, U_{in} ($t < 5$ ms) is approximated by a linear ramp. No symmetry condition is forced along the slits midline. The computations are performed on grids with $N_x = 1{,}024$ and $N_z = 256$ and the time step is adjusted so that the CFL is of order 10^{-2}.

A subroutine is added to the numerical code in order to track the vortex dipoles as they move along the channel. Vortex dipole tracking can be achieved through a systematic monitoring of local maxima and minima in speed and pressure. A vortex dipole is located where the pressure field and the streamwise component of the velocity field have a local maximum surrounded by two local minima.

5 Results

The results obtained in this study are organized as follows; first, we give an integrated account of the phenomena we have observed in our laboratory and numerical experiences (Sect. 5.1) and then we provide a quantitative description of the properties of the observed vortex dipolar structures (Sect. 5.2).

5.1 Flow development

In order to provide the reader with a general idea of the sequence of events in a prototype case, Fig. 5 shows five frames illustrating (a) the formation of the Starting Vortex Dipolar structure (SVD) at the first slit, (b) the birth of the second-slit SVD, (c) the generation of the sequence of Trailing Vortex Dipolar structures (TVDs) in the core of the first-slit jet, (d) the first-slit SVD squeezing through the second slit, and (e) the shedding of Boundary Vortex Dipolar structures (BVDs) from the rear part (or upstream face) of the boundaries defining the second constriction. These numerical results correspond to a configuration with $h_1 = 1$ mm, $h_2 = 2$ mm, $L = 20$ mm and $Re = 900$, so that the peak jet velocity through the first slit is of 15 m/s (the minimum typical velocity of the glottal jet at the vocal folds).

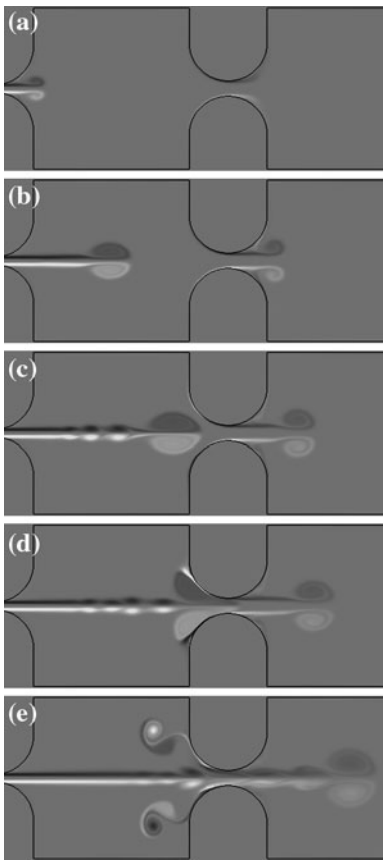

Fig. 5 Sequence showing the numerical vortex dipolar structures in the prototype configuration ($h_1 = 1$ mm, $h_2 = 2$ mm, $L = 20$ mm and $Re = 900$) at **a** 3.5 ms, **b** 5.8 ms, **c** 7.2 ms, **d** 7.9 ms and **e** 9.5 ms

A zoom on the dipolar head of the jet formed at the first slit from the Schlieren pictures and from the numerical simulations is provided in Fig. 6. An estimation of the position of the centroids of the laboratory SVDs (and of the distance d between them) can be achieved from a weighted average in intensity performed in the region where the structures are visible. The radius a of the circular area containing the laboratory SVDs can also be extracted from the images. Figure 7 shows vorticity, streamwise velocity and pressure profiles along the line joining the centroids of the dipolar head formed at the first slit in the numerical simulation. The dipole center is associated with a local maximum in pressure, while the dipole centroids can be located using the local minima in pressure. The radius a of the dipolar structure can be estimated from the zeros of the vorticity profile across the dipole.

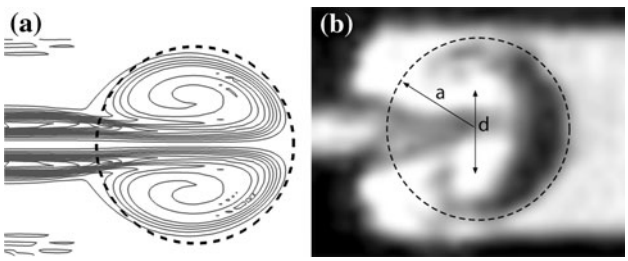

Fig. 6 The spiraled pattern formed by the iso-vorticity contours of the numerical first-slit starting vortices (**a**) and by the mushroom-shaped laboratory structure visualized with the Schlieren technique, inscribed in a *dashed circle*

The formation time scale and the initial size of the leading dipolar structures depend on the slit width. The second-slit jet is born at the same time as the first-slit jet if the consecutive slits are equally constricted, i.e. if $h_1 = h_2$ (see Fig. 8). For the prototype configuration in the target problem ($h_1 < h_2$), jet formation is not exactly simultaneous: at the second slit, the flow velocity is lower and vorticity formed by flow separation takes longer to detach from the wall. Once formed, the dipolar heads grow in size as they progress along the channel preserving the ratio between the centroid separation d and the radius a for a certain time.

Both jets develop a finite series of progressively smaller vortex dipoles (of about the size of the jet core) that follow the leading dipolar head. These structures are correlated with a varicose jet mode which develops before the first-slit jet traverses the second slit. The numerical simulations show that these small dipoles evolve with a leapfrogging dynamics.

The varicose-like mode, which settles first, tends to evolve into a sinuous-like instability. This is probably favoured by the jet velocity profile at the neck of the second slit, which evolves from a smoothed top hat initial profile to a parabolic profile. The varicose instability is characteristic of planar jets with flat exit mean velocity profiles, while parabolic profiles lead to the dominance of the sinuous instability. With the sinuous-like mode, the jet core–sized sequence of symmetric dipoles associated with the jet start tilting, moving away from the common axis. When the instability reaches the front of the jet, the leading dipole also twists and bends in a zigzag fashion. This meandering behavior, typical of long injection times

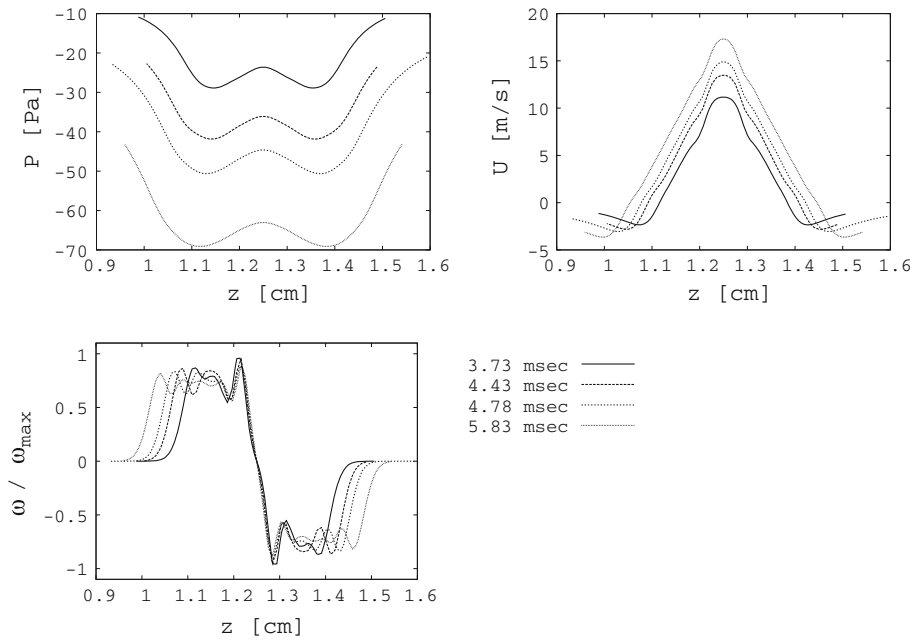

Fig. 7 Sequence of profiles of pressure, streamwise velocity and vorticity for cross-sections defined along the line uniting the first-slit starting vortex dipolar centroids in the numerical simulations

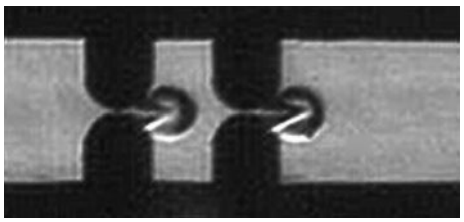

Fig. 8 Formation of vortex dipolar structures observed in the laboratory for a channel with two consecutive 1-mm-wide slits

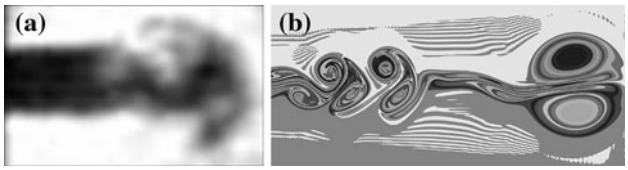

Fig. 9 Sinuous-like instability observed **a** in the laboratory visualizations and **b** in the numerical iso-vorticity contours

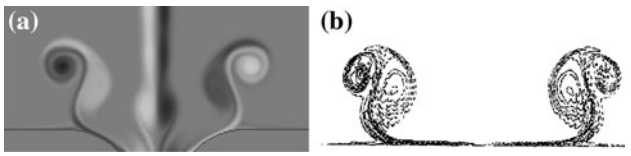

Fig. 10 Vorticity field obtained **a** when the first-slit jet traverses the second slit, and **b** when a vortex dipole impinges on a flat non-slip wall in Orlandi (1990)

(Afanasyev and Korabel 2004), is illustrated in Fig. 9. Although the overall behavior of the in vitro and in silico jets remains comparable, the jet core–sized dipoles are not resolved by our Schlieren visualizations.

Let us focus on the phenomena observed in the ventricle, i.e. in the region of the model between the two slits. When the dipolar head of the first-slit jet squeezes through the second slit, specular pairs of vortex dipoles of intermediate size are shed from the two upstream faces of the semi-cylinders defining the second constriction (see Fig. 5e). The shape and dynamics of these structures closely resemble those observed (experimentally and numerically) by Orlandi (1990) for a vortex dipole impinging against a non-slip flat boundary (see Fig. 10). Such vortex dipoles can be seen as a result of a 'rebounding' mechanism taking place as the series of vortex dipoles associated with the first-slit jet interact with the non-slip boundaries defined by the sides of the liplike constriction. After rebounding, BVDs describe curved trajectories in the upstream direction ($-x$) at relatively low speeds, interacting collectively with the jet and the ventricular walls. The dipolar nature of these patterns is clearer in the numerical simulations than in the Schlieren experiments. However, the correspondence between numerical and laboratory structures at this stage of the flow evolution is still

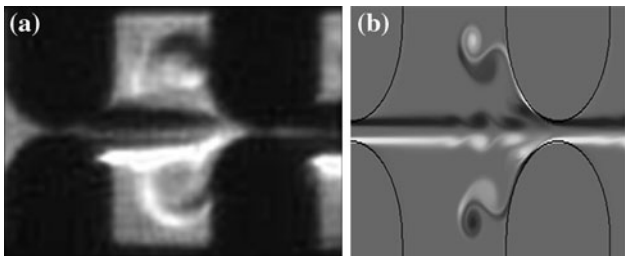

Fig. 11 Laboratory (**a**) and numerical (**b**) vortex dipolar structures in the ventricle after the passage of the first-slit jet through the second slit

apparent. A comparison between the laboratory and numerical results in the milliseconds following the passage of the first-slit jet through the second slit is given in Fig. 11. The complex process contributes to forming relatively large and persistent vortical structures of opposite sign accumulating in either side of the jet within the ventricle.

After this stage, the laboratory coherent structures break down and a 3D turbulent state follows. As expected, purely 2D (numerical) vortex dipoles are longer-lasting than the initially quasi-planar laboratory structures. The turbulent state is attained at most after 50 ms.

To sum up, our investigations account for the generation of three types of vortex dipolar structures for the flow that develops in these geometrical configurations and inflow conditions:

- large-size, unstable Starting Vortex Dipolar structures (SVDs) generated at the slits representing the true and the false vocal folds in the larynx,
- midsize structures created by the interaction of vorticity with the solid boundaries, that we classify as Boundary Vortex Dipoles (BVDs), and
- small size Trailing Vortex Dipolar structures (TVDs) emerging sequentially in the trailing jet and exhibiting a complex dynamics.

5.2 Properties of the vortex dipolar structures

Let us first consider some details of the large-size SVDs. The dipolar head starts translating after an initial period when it mainly grows absorbing the jet from the nozzle. Figure 12 shows the evolution of the streamwise coordinate of the centers, of the radius a and the distance d for the laboratory and the numerical SVDs generated at the neck of the second slit for the prototype case. The Schlieren videos allow us to perform a visual assessment of the vortex dipolar structures. A manifest proportionality is found between the Schlieren images and the modulus of the vorticity field, which can be explained by the twin evolution of vorticity and concentration. Both vorticity and

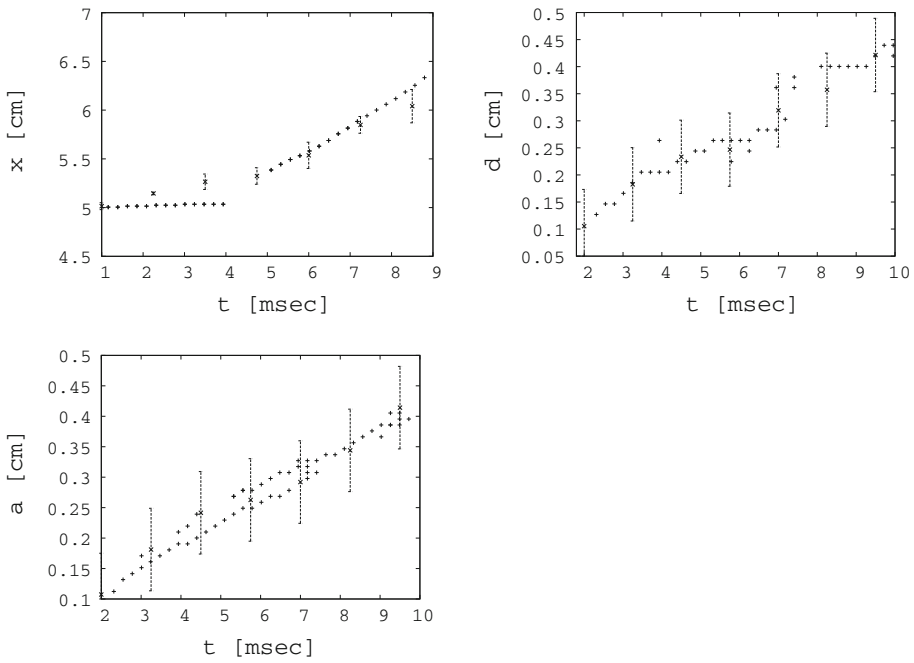

Fig. 12 Translation (x, above) and growth (a, d, below) of the second-slit starting vortex dipolar structure in the prototype configuration. *Crosses* correspond to the data extracted from the Schlieren images and pluses to numerical data

Helium concentration in the Schlieren images are correlated and governed by the convective diffusion phenomenon, but they have different diffusion coefficients. In agreement with this difference, the size of the laboratory structures is found to be 4.6 times larger than the numerical structures. The experimental data in Fig. 12 have been shifted down to show that the size and distance between centroids evolve in agreement with the numerical data.

A general trend that we have remarked for the SVDs is that the ratio d/a during the first milliseconds is found to be approximately constant and close to 1. In Fig. 13, we show d versus a for the second-slit SVD of the prototype case. The points lie approximately on a line that can be fitted with a slope of (0.90 ± 0.08). The dipolar head grows preserving d/a during about 7 ms, when the ratio starts falling (notice that the last point in Fig. 13 already starts deviating from the straight line). This property is lost earlier in time when the second slit is widened, i.e. for $h_2 = 4$ mm and $h_2 = 6$ mm.

Afanasyev (2006) shows that once the vortex dipole is already formed at the nozzle and starts translating, the ratio of its speed of propagation to the mean velocity of the jet has a universal value of 0.5, which holds for a 2D flow induced by a jet ejected from a square-edged nozzle of finite size. If we compute this ratio with the data extracted from numerical simulations without a second slit and for a certain temporal range after the startup time ($7 \text{ ms} < t < 14 \text{ ms}$), this ratio is found to be 0.49. This value is very close to the universal ratio found by Afanasyev, even if the slit representing the folds that we are using is round shaped and in spite of the presence of the core-sized TVDs, which are absent in Afanasyev's model.

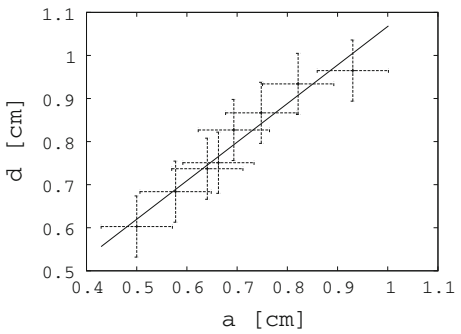

Fig. 13 Distance between the laboratory starting vortex dipolar centers d as a function of the radius a of the head leaving the second slit for $h_2 = 2$ mm

Let us also mention that, in line with Afanasyev's results and in contrast with what is reported for vortex rings, no pinch off is observed for the SVDs in our experiments: the dipolar head remains attached to the trailing jet.

Figure 14 shows space-time plots of the streamwise velocity maxima (monitored to track the center of the vortex dipoles). The motion of the dipolar head is well approximated by a quadratic law next to the nozzle that has emitted it and while the valve is being opened. Afterwards, the motion of the dipolar head is linear in average. The sequence of lines below the dipolar head trajectory correspond to the sequential emerging of TVDs. Merging of these TVDs with the leading structure affects the pace of the latter, making its progression less regular. The space-time plots show the three types of vortex dipolar structures for two aperture values of the second slit. The horizontal lines correspond to the maxima associated with the first- and

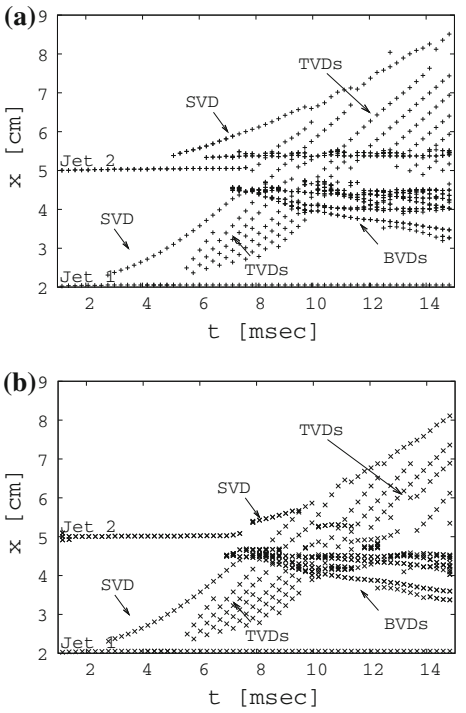

Fig. 14 Streamwise location (x) of the streamwise velocity maxima (U_{max}) monitored to track the center of the vortex dipolar structures for two geometrical configurations with second slits of different widths: **a** $h_2 = 2$ mm and **b** $h_2 = 4$ mm. *Labels* in the *plots* indicate the maxima associated with the following: first-slit jet (Jet 1), the second-slit jet (Jet 2), the trajectory of the head of each Starting Vortex Dipolar structure (*SVD*), the series of Trailing Vortex Dipolar structures (*TVDs*) and the group of Boundary Vortex Dipolar structures (*BVDs*)

second-slit jets. The BVDs created when the first-slit jet traverses the second slit ($2\text{ cm} < x < 5\text{ cm}$) have a streamwise position indicated by the negative slope lines. Notice that, with respect to the TVDs evolving in the core of the first-slit jet, the sequential TVDs of the second-slit jet are generated at about half the frequency. When the second slit is widened ($h_2 = 4$ mm and $h_2 = 6$ mm), the average translation speed of the dipolar head past the second slit grows accordingly: 2.9 m/s for $h_2 = 2$ mm, 3.7 m/s for $h_2 = 4$ mm, 4.8 m/s for $h_2 = 6$ mm.

6 Conclusions

This paper shows that the starting airflow in a channel with two consecutive slits is dominated by a double jet dynamics in which it is possible to identify vortex dipolar structures (counter-rotating line vortex pairs) of different size and origin. The fluid dynamical problem that we discuss is a simplified version of laryngeal flow at the onset of voice production. Because the geometry that we study is static and schematic, we do not claim that the dynamics that we visualize is transposable to the real voice generation mechanism.

Our study combines high-speed imaging of Schlieren flow visualizations and Direct Numerical Simulations of the full channel. The double-slit model is mounted so that the length of the slits is parallel to the optical rays of the Schlieren system. This configuration is optimal if the flow that is studied maintains a certain spatial coherence along the direction defined by the length of the slits. This coherence is enhanced in our experiment by the twofold condition in space and time provided by the geometrical configuration (a relatively short distance separating two aligned slits) and by the focus on the (short) times which are relevant for voice onset. False vocal fold-like structures do not only straighten the glottal jet flow as indicated by many authors, but also reinforce the quasi-two-dimensionality of the flow, at least during the times following flow onset.

Three types of Vortex Dipolar structures (VDs) are disclosed by our experiments: large-size starting VDs formed at the slits, midsize boundary VDs generated by the interaction of vorticity with the walls, and series of small size trailing VDs emerging in the stem of the dipolar heads with the onset of instabilities in the shear layers. The VDs that we observe suffer accelerations, expansion and different kinds of interactions: mutual interactions, interactions with the trailing jet or interactions with the solid boundaries. The latter can be described as 'reboundings' in the sense introduced by Orlandi. Both varicose (symmetric) and (asymmetric) sinuous-like instabilities may affect the dynamics of the VDs associated with the jets. The interplay of boundary VDs in the ventricle results in a rather persistent configuration of opposite-sign vorticity patches at either side of the jet. Laboratory experiments are in progress to gain further insight into the dynamics of vortex structures in less ideal conditions and beyond flow onset.

Acknowledgments This research has been partially supported by the project SticAmSud 07STIC-05.

References

Afanasyev YD (2006) Formation of vortex dipoles. Phys Fluids 18:037103

Afanasyev YD, Korabel VN (2004) Starting vortex dipoles in a viscous fluid: asymptotic theory, numerical simulations, and laboratory experiments. Phys Fluids 16(11):3850–3858

Agarwal M, Scherer RC, Hollien H (2003) The false vocal folds: shape and size in frontal view during phonation based on laminagraphic tracings. J Voice 17:97–113

Bailly L, Pelorson X, Henrich N, Ruty N (2008) Influence of a constriction in the near field of the vocal folds: physical modeling and experimental validation. J Acoust Soc Am 124(5):3296–3308

Billon A, Valeau V, Sakout A (2005) A combined lda and flow-visualization study on flue organ pipes. J Fluids Struct 21:121–132

Cremer L, Ising H (1967-1968) Die selbsterregten Schwingungen von Orgelpfeifen. Acustica 19(3):143–153

Deverge M, Pelorson X, Vilain C, Lagrée PY, Chentouf F, Willems J, Hirschberg A (2003) Influence of collision on the flow through in-vitro rigid models of the vocal folds. J Acoust Soc Am 114(6):3354–3362

Erath BD, Plesniak MW (2006) The occurrence of the Coanda effect in pulsatile flow through static models of the human vocal folds. J Acoust Soc Am 120(2):1000–1011

Erath BD, Plesniak MW (2006) An investigation of bimodal jet trajectory in flow through scaled models of the human vocal tract. Exp Fluids 40(5):683–696

Erath BD, Plesniak MW (2006) An investigation of jet trajectory in flow through scaled vocal fold models with asymmetric glottal passages. Exp Fluids 41:735–748

Glesser M, Valeau V, Sakout A (2008) Vortex sound in unconfined flows: application to the coupling of a jet-slot oscillator with a resonator. J Sound Vib 314:635–649

Gutmark EJ, Grinstein FF (1999) Flow control with noncircular jets. Ann Rev Fluid Mech 31:239–272

Hofmans GCJ (1998) Vortex sound in confined flows. Eindhoven University, Eindhoven, p 233

Hofmans GCJ, Groot G, Ranucci M, Graziani G, Hirschberg A (2003) Unsteady flow through in-vitro models of the glottis. J Acoust Soc Am 113(3):1658–1675

Howe MS (1998) Acoustics of fluid-structure interactions. Cambridge University Press, Cambridge

Howe MS (2003) Theory of vortex sound. Cambridge University Press, Cambridge

Howe MS (2007) Hydrodynamics and sound. Cambridge University Press, Cambridge

Huang JM, Hsiao FB (2006) On the mode development in the develping region of a plane jet. Phys Fluids 11(7):1847–1857

Khosla S, Muruguppan S, Gutmark E, Scherer R (2007) Vortical flow field during phonation in an excised canine larynx model. Ann Otol Rhinol Laryngol 116:217–228

Kucinschi BR, Scherer RC, DeWitt KJ, Terry TM (2006) Ng flow visualization and acoustic consequences of the air moving through a static model of the human larynx. J Biomech Eng 128:380–390

Liepmann D, Gharib M (1992) The role of streamwise vorticity in the near-field entrainment of round jets. J Fluid Mech 245:643

Neubauer J, Zhang Z, Miraghaie R, Berry DA (2007) Coherent structures of the near field flow in a self-oscillating physical model of the vocal folds. J Acoust Soc Am 121(2):1102–1118

Orlandi P (1990) Vortex dipole rebound from a wall. Phys Fluids A 2(8):1429–1436

Paál G, Angster J, Garen W, Miklós A (2006) A combined lda and flow-visualization study on flue organ pipes. Exp Fluids 40(6):825–835

Pelorson X, Hirschberg A, Hasselt RV, Wijnands A, Auregan Y (1994) Theoretical and experimental study of quasisteady-flow separation within the glottis during phonation. Application to a modified two-mass model. J Acoust Soc Am 96(6):3416–3431

Sciamarella D, Le Quéré P (2008) Solving for unsteady airflow in a glottal model with immersed moving boundaries. Eur J Mech B Fluids 27(1):42–53

Settles G (2001) Schlieren and shadowgraph techniques, visualizing phenomena in transparent media. Springer, Berlin

Triep M, Brucker Ch, Schroder W (2005) High-speed PIV measurements of the flow downstream of a dynamic mechanical model of the human vocal folds. Exp Fluids 39:232–245

Verge MP, Fabre B, Mahu WEA, Hirschberg A, van Hassel RR, Wijnands APJ, de Vries JJ, Hogendoorn CJ (1994) Jet formation and jet velocity fluctuations in a flue organ pipe. J Acoust Soc Am 95:1119

Vilain CE (2002) Thèse de Doctorat signal, image, Parole Télécommunication. Institut National Polytechnique de Grenoble, France, p 193

Wilson TA, Beavers GS, DeCoster MA, Holger DK, Regenfuss MD (1971) Experiments on the fluid mechanics of whistling. J Acoust Soc Am 50(1B):366–372

Zheng X, Bielamowicz S, Luo H, Mittal R (2009) A computational study of the effect of false vocal folds on glottal flow and vocal fold vibration during phonation. Ann Biomed Eng 37(3):625–642